AIAA JOURNAL
Vol. 44, No. 3, March 2006

Control of High-Frequency Thermoacoustic Pulsations by Distributed Vortex Generators

Christian Oliver Paschereit*
Berlin University of Technology, 10623 Berlin, Germany
and
Ephraim J. Gutmark†
University of Cincinnati, Cincinnati, Ohio 45221-0070

Axisymmetric and helical instabilities modes were identified in an experimental combustor. The low-frequency instabilities were associated with the external recirculation zone downstream of the dump plane and the central recirculation zone formed by vortex breakdown. High-frequency helical instabilities were excited by the small-scale vortices that were shed at the initial separating shear layer at high-power levels. Miniature vortex generators were installed at the circumference of the burner's exit to interfere with the rollup of these vortices through the induction of streamwise vorticity. The tests showed that, in addition to the effect on the initial vortices, the process that leads to the formation of large-scale vortices through pairing and vortex merging was disrupted. Thermoacoustic instabilities that are excited by the periodic heat release due to the presence of coherent vortices were, thus, avoided in both the high- and low-frequency ranges. The effect was particularly significant in the high-frequency oscillations that reached high-amplitude level in the baseline burner and were suppressed by up to 28 dB by the miniature vortex generators. At the same time, low-frequency instabilities were reduced by 50%. Emissions of NO_x were reduced by a factor of two in a wide range of operating conditions. The results obtained in the laboratory combustor operating at atmospheric pressure were also confirmed in high-pressure combustion tests.

Introduction

DURING the past decade, the drive for lower emissions of oxides of nitrogen in stationary gas turbines has led to the widespread use of lean premix burners and convectively cooled combustion chambers. These technological changes have resulted in a reduced stability of flame anchoring and lower acoustic damping. Consequently, modern gas turbines are more susceptible to combustion-driven oscillations and the importance of controlling thermoacoustic phenomena in gas turbine combustors has increased.

The stability characteristics and emissions of gas-turbine combustors are determined by flow dynamics that govern the mixing between fuel and air and between hot reaction products and fresh mixed reactants. In a swirl-stabilized combustor with a sudden expansion region, the relevant flow dynamics include coherent vortices evolution in the separating shear layer at the sudden expansion and vortex breakdown near the axis that provides the central recirculation zone. The formation of coherent structures in the separating shear layer is initiated by Kelvin–Helmholtz instability. The exponential growth of the velocity and vorticity perturbations leads to a nonlinear process that eventually causes the roll-up of the shear layer into vortices. The initial vortex-shedding frequency f_i, which is also called the most amplified frequency, is determined by the characteristics of the exit velocity profile. These vortices are typically small and are associated with high-frequency oscillations. The initial vortices grow in the shear layer and interact as they are convected downstream. In controlled laboratory tests, the shear layer grows through a pairing process. At high Reynolds numbers and less controlled flows, the interaction is more complex and involves production of small-scale turbulence. Because of these vortex interactions and entrainment, the shear layer spreads, and the frequency associated with the large vortices decreases. These larger-scale coherent structures control the entrainment and mixing processes and may excite low-frequency acoustic instabilities when they match the combustion chamber acoustic resonance modes.[1]

In reacting flows, the interaction between large-scale coherent structures, acoustic resonant modes, and the heat release process was shown to cause undesired thermoacoustic instabilities. By the domination of the mixing process, coherent vortices also control combustion efficiency and emissions. Realizing the important role of large scale structures in the combustion process, researchers developed passive and active methods to control the vortical structures in the flow.[2–4] Passive control strategies apply special combustor design to enhance small-scale mixing, to reduce the coherence of large-scale vortices, and to generate axial vorticity. Noncircular geometry, vortex generators, and other modifications in the inlet nozzle design have been the topics of extensive research in the past 15 years as reviewed by Gutmark and Grinstein.[5] Of specific relevance to this paper is McManus and Bowman's[6] work where the effect of delta wing vortex generators (VGs) on combustion instability in a sudden expansion two-dimensional dump combustor was investigated. They observed that the streamwise vorticity introduced by the VGs increased the three dimensionality of the large-scale structure in the separating shear layer resulting in reduced low-frequency pressure fluctuation levels.

The present paper describes an experimental investigation on the utilization of distributed miniature VGs to enhance the performance of a low-emission swirl-stabilized combustor. The tests were initially performed in a model combustor at atmospheric conditions and then extended to high-pressure conditions in a gas-turbine engine. When the acoustic boundary conditions and operational parameters were adjusted, the combustor exhibited instability modes at high and low frequencies. Miniature VGs were installed at the burner's exit. This passive control technique was shown to be effective in the suppression of low- and high-frequency modes of thermoacoustic instabilities and at the same time reduced NO_x, CO, and unburned hydrocarbon (UHC) emissions in a wide range of operating conditions.

Received 1 July 2002; accepted for publication 16 November 2005.

*Professor, Hermann-Föttinger-Inst. of Fluid Dynamics; oliver.paschereit@tu-berlin.de. Member AIAA.

†Professor, Department of Aerospace Engineering and Engineering Mechanics; Ephraim.Gutmark@uc.edu. Associate Fellow AIAA.

The paper describes the effect of the VGs on the unstable mode structure and combustor performance.

Experimental Setup

Combustion Facility

The combustion facility is shown in Fig. 1. The test rig consists of a plenum chamber upstream of the swirl-inducing burner and a combustion chamber downstream of the burner. The burner, which is described in detail by Doebbeling et al.,[7] induces swirling flow in the combustion chamber with an initial swirl number $S = 0.7$. The flow Reynolds number was 8×10^4, and the boundary layer $Re = 3.5 \times 10^3$. The details on the flowfield produced by this burner were described by Paschereit et al.[4] The plenum chamber contains perforated plates to reduce the turbulence level of the flow. The circular combustion chamber consists of an air-cooled double-wall quartz glass to provide full visual access to the flame. The exhaust system is an air-cooled tube with the same cross section as the combustion chamber to avoid acoustic reflections at area discontinuities. The acoustic boundary conditions of the exhaust system could be adjusted from almost anechoic (reflection coefficient $|R_f| < 0.15$) to open-end reflection. To induce thermoacoustic instability that will have moderately high amplitude as required for testing, the combustor exhaust was fitted with a large opening that provided a reflection coefficient of $|R_f| > 0.7$. The natural gas flame was stabilized in a recirculation region near the swirl-generating burner's outlet. The burner was operated at atmospheric conditions. Flow visualization tests were conducted in a water tunnel facility described by Paschereit et al.[4]

Pressure fluctuations were measured using Brüel and Kjær (B&K) water-cooled microphones. The wall-mounted water-cooled $\frac{1}{4}$-in. (6.35-mm) condenser microphones were placed at an axial distance of $x/D = 2.5$. The holders consisted of a small orifice ($d = 1$ mm) open to the combustion chamber. The microphone diaphragm was placed in a small cavity and was heat radiation protected. The resonance frequency of the holder was larger than $f_{\text{res}} > 20$ kHz. Using condenser microphones rather than piezoelectric pressure probes gave the advantage of highly accurate data in phase and amplitude necessary for acoustic measurements. The frequency response of the microphones in probe holders was compared against standard B&K microphones and showed good agreement. The microphones were calibrated using a B&K Pistonphone calibrator. Tests were performed in a wide range of operating conditions including varying the power output level, the combustion air preheating temperature, and the equivalence ratio. The operating conditions were normalized by the corresponding values at the standard operating conditions: power P_n, preheating temperature T_n, and air excess ratio (inverse of equivalence ratio) λ_n, where the subscript n refers to the nominal or reference operating conditions. The test matrix included the following conditions: 1) varying power in the range of $1 < P/P_n < 1.43$ at nominal normalized air excess ratio λ_n and nominal preheating temperature of T_n, 2) varying the preheating temperature in the range of $0.75 < T/T_n < 1.25$ at λ_n and a power of $P/P_n = 1.25$, and 3) varying the air excess ratio λ in the range of $0.87 < \lambda/\lambda_n < 1.11$ at nominal power P_n and nominal preheating temperature T_n.

The operating conditions of the burner have been maintained by analyzing the exhaust gas composition using a physical gas analysis system. CO and CO_2 have been analyzed by using nondispersive infrared spectroscopy. The nitric oxides NO and NO_2, combined in NO_x, have been detected with a chemiluminescence analyzer. The detection of the remaining O_2 in the exhaust gas was made utilizing the paramagnetic properties of oxygen in the analyzing device. Carbon and oxygen balances were continuously computed, and agreement within 0.2% was assured. The system was calibrated daily with calibration gases.

Heat Release Measurements and Visualization System

Time-varying heat release was recorded with two filtered fiber optic probes to detect OH radiation. Several studies have shown that OH appears in superequilibrium concentrations in the flame front region.[8] Therefore, the OH emissions were used as a qualitative indicator to detect the heat release at the active combustion regions. The signal was bandpass filtered with low and high cutoff wavelengths of 290 and 390 nm. The circular field of view of the probes had a diameter of $d = 10$ mm at the flame position. The probe was coupled with a photomultiplier with a response time of 1 ns. The probes monitored the upper shear layer ($r/D = 0.5$) and the combustor centerline at an axial distance $x/D = 0.514$ downstream from the dump plane. The probes were also used to measure radial cross correlations of the OH signals.

Results and Discussion

Instability Structure

Several thermoacoustic unstable modes were observed in the combustor during nominal and offdesign operation. During nominal operation at a power output of 500 kW and lean fuel/air mixture, two low-frequency modes were detected: an axisymmetric mode at a Strouhal number $Sr = fD/U$, of 0.58 and a helical mode at a $Sr = 1.16$. D is the burner exit diameter, and U the average mean velocity. The mode at $Sr = 0.58$ matched the longitudinal acoustic mode of the combustion chamber. The spectra of the pressure and OH fluctuations in the burner's shear layer and along its centerline are shown in Fig. 2 at the nominal operating conditions. The level of the various unstable modes varies along the radius of the combustor and particularly across the shear layer. The spectra shown here are at a particular radial location and represent typical behavior but not the amplitude of the instabilities across the entire shear layer. At this particular point, the shear layer OH spectrum shows a weak instability mode at a frequency of $Sr = 0.58$, a strong one at a frequency of $Sr = 1.16$, and low amplitude peaks at $Sr = 2.66$ and 7.77. Paschereit et al.[4] showed that the $Sr = 0.58$ axisymmetric mode is excited at the outer edge of the shear layer, between the swirling jet and the external recirculation zone at the sudden expansion. The higher $Sr = 1.16$ helical mode is driven at the inner shear layer between the jet and the central recirculation zone formed by vortex breakdown. The OH spectrum measured along the centerline shows low-level peaks at all of these frequencies. When the axisymmetric mode couples with the longitudinal acoustic mode of the combustor, it causes a one-dimensional pressure wave that

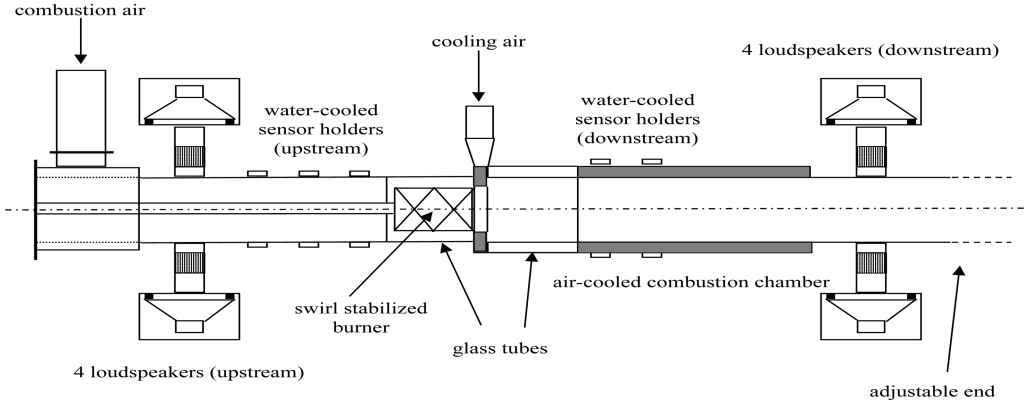

Fig. 1 Experimental arrangement of the atmospheric combustion rig.

affects the entire cross section of the combustor. It is, thus, expected that its imprint will be seen also in the centerline spectrum. The presence of high-level peaks in the shear layer OH spectrum rather than along the centerline may indicate that the sources of the instabilities are combustion within the vortices in the shear layer. However, as indicated by the pressure spectrum, not all of the heat release fluctuations coupled with the acoustic modes of the combustor to produce high-level pressure oscillations.

The mode structure of the different unstable modes was assessed from the radial cross correlations between OH chemiluminescence radiation measured at two radial points in the combustion chamber by two filtered fiber optic probes. One of the probes was stationary at the upper shear layer of the incoming flow at an axial distance of $x/D = 0.086$ from the dump plane. The other probe was moved radially starting from the stationary probe ($r/D = 0$) until it reached the opposite shear layer. The results are shown in Fig. 3, in which the

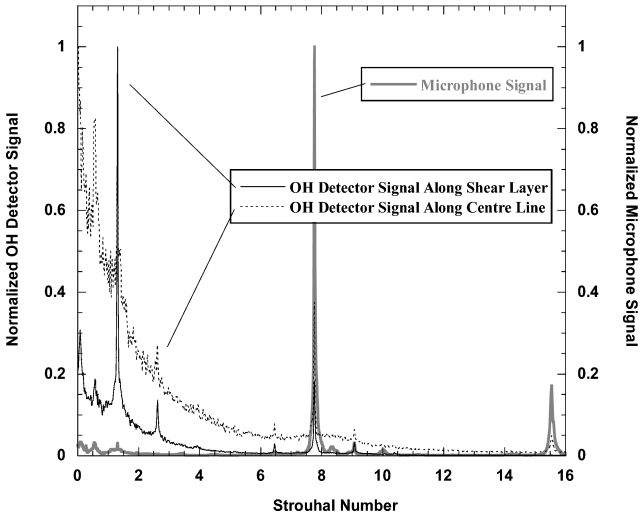

Fig. 2 Pressure and OH spectra along shear layer and centerline at nominal power and equivalence ratio.

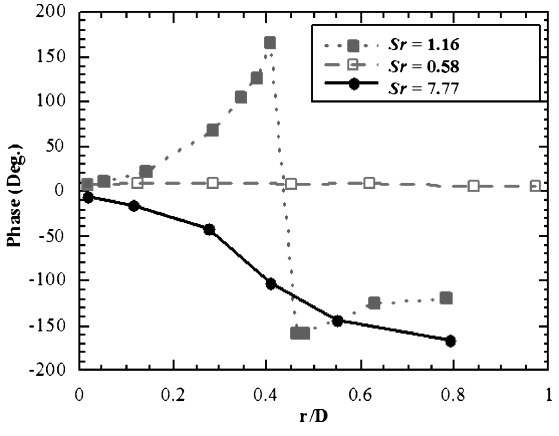

Fig. 3 Phase difference of the OH cross correlations as function of radial distance; cross correlations for three different instabilities.

relative phase angle between the two OH signals is plotted as a function of r/D. The instability mode at $Sr = 1.16$ underwent a phase change of 180 deg corresponding to a helical mode, whereas the axisymmetric mode $Sr = 0.58$ remained at a zero phase angle across the combustor. For offdesign operating conditions that included increased power by up to 43% above standard level, or reduced air inlet temperature by up to 25% below standard conditions, an additional high-frequency helical mode was excited at a $Sr = 7.77$. The pressure spectrum indicates particularly high amplitude at $Sr = 7.77$ and a low-level peak at the first harmonic of this frequency. When the high-frequency instability reached its limit cycle, it dominated the thermoacoustic modes and the lower frequencies were not excited in spite of the relatively strong peaks of heat release at these frequencies.

Unlike the large-scale vortices at Sr of 0.58 and 1.16, the excitation of the high-frequency unstable mode can be attributed to the small-scale vortices that were produced at the burner's exit by the Kelvin–Helmholtz instability (see Ref. 9). These vortices scale with the initial separating shear layer thickness, which is determined by the thickness of the circumferential boundary layer inside the burner upstream of the sudden expansion. Paschereit et al.[10] showed that when the Strouhal number of a jet, which is based on the initial momentum thickness, $Sr_\theta = \omega\theta/U$, where ω is the angular frequency and θ is the initial momentum thickness, is in the range between $Sr = 0.15$ and 0.25, the jet flow is unstable. In the present case, with an initial momentum thickness of $\theta = 7.5 \times 10^{-4}$ m, $Sr_\theta = 0.21$, which is within the aforementioned range.

The vortex shedding at the burner's exit lip was visualized in a water tunnel (Fig. 4). The instantaneous images of the vortex were captured at different phases during its formation, revealing a strong coherent structure despite the high swirl number. In reacting flow, as these coherent structures evolve from small incipient vortices at the burner's lip to large-scale vortices in the shear layer, they mix fuel, air, and combustion products and, thus, dominate the pattern of heat release. The subsequent interaction between heat release and acoustic pressure waves set up the conditions that can lead to stable or unstable thermoacoustic behavior of the combustor. In the present case, the high-frequency unstable mode that became excited, were visualized using an intensified and filtered charge-coupled device camera, which was triggered at different phase angles relative to the unsteady pressure signal. When this technique was used, phase-averaged OH images were obtained for different thermoacoustic instabilities. A helical unstable structure was observed at the high-frequency mode of $Sr = 7.77$ (Fig. 5). Unlike the axisymmetric mode, which exhibited a variable combustion intensity during one cycle of instability, while maintaining a symmetric structure, this helical mode maintained a constant intensity level with circumferential variation of the maximum heat release location. The high light intensity shifted from the upper shear layer at 0 deg to the lower shear layer at 180 deg. The integration of the light intensity over the upper and the lower half of the flame during a full cycle shows clearly the antisymmetry of the structure and the phase shift of 180 deg in heat release of the upper and lower half of the flame (Fig. 5b).

VGs for Suppression of High-Frequency Instabilities

The strategy pursued here to prevent the high-frequency thermoacoustic instability was to disrupt the formation of the small vortices at the burner's exit that were driving this mode. To achieve that, it

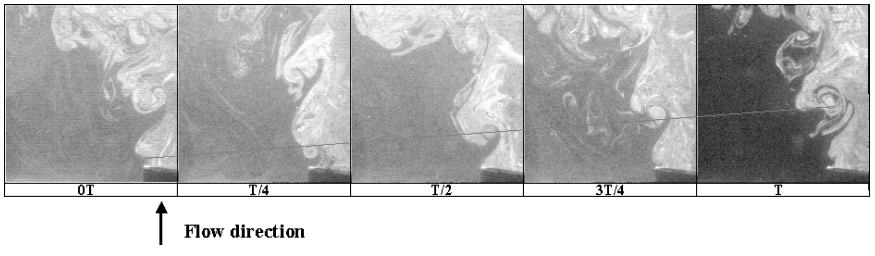

Fig. 4 Water-tunnel visualization of evolution of small-scale vortices at dump plane.

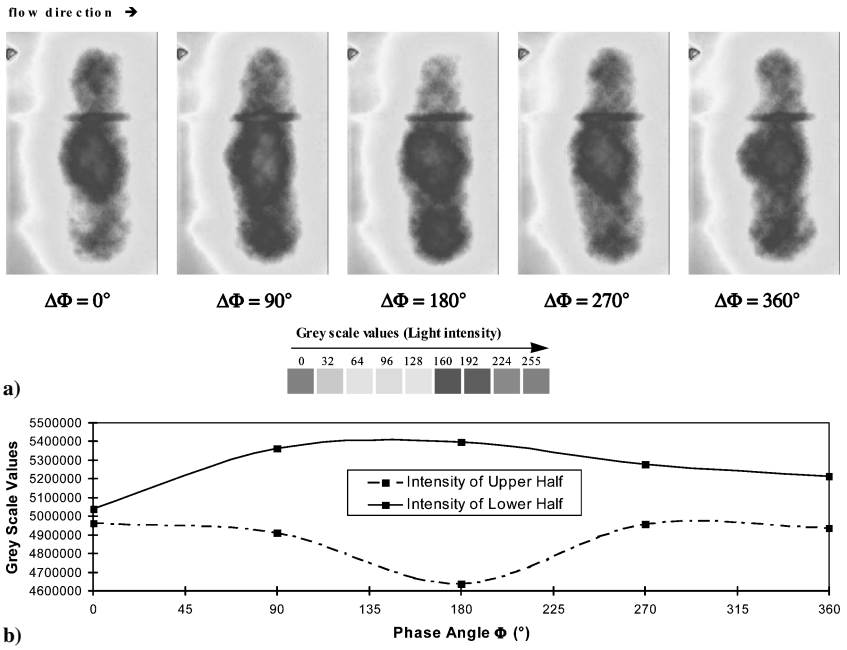

Fig. 5 High-frequency instability at $Sr = 7.77$: a) phase-averaged visualization at various phase angles and light intensity of flame and b) integrated light intensity over upper and lower half of flame at various phase angles.

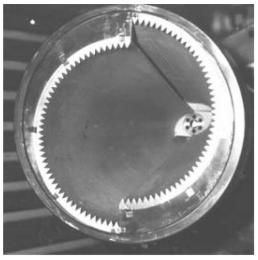

a) Shark-teeth configuration

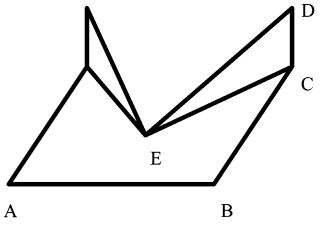

VG size	Length A–B	Length B–C	Length C–D	Length C–E
Large	30 mm	30 mm	15 mm	26 mm
Small	20 mm	20 mm	10 mm	17.3 mm

b) Geometry of vortex generators

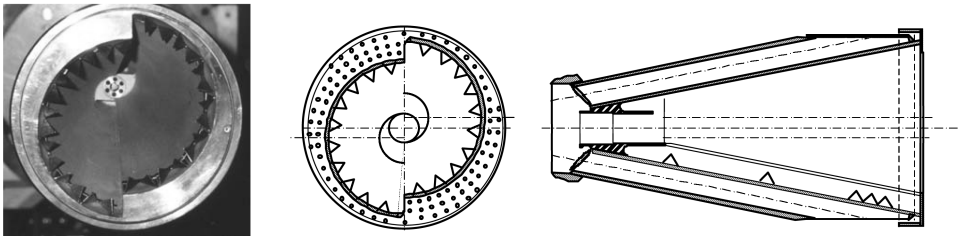

c) Arrangement of vortex generators at slots and burner exit

Fig. 6 Arrangement and dimensions of VGs.

was necessary to interfere with the circumferential uniformity of the boundary-layer thickness and to break the coherence of the vortices that are shed at the burner's lip. Miniature VGs were installed circumferentially at the burner's exit to perturb the formation of the initial shear layer. The geometry and dimensions of the different VGs are shown in Fig. 6. The VGs were primarily designed to suppress the high-frequency instabilities of $Sr = 7.77$, but some tests were performed to assess their impact on the low-frequency instability of $Sr = 0.58$. The possible effect on the low-frequency relied on the assumption that the perturbation to the initial shear layer can also disrupt the chain of vortex interactions, which eventually leads to the formation of large-scale vortices. Periodic heat release caused by these vortices was determined to be a cause for combustion instabilities at the low-frequency range.[11]

The pressure and OH spectra of the burner equipped with the miniature VGs at the baseline operating conditions are shown in Fig. 7. The miniature VGs reduced the level of the peak pressure fluctuations at the high frequency by over 25 dB relative to the baseline burner. At the same time, the low-frequency instability at $Sr = 0.58$ and its first subharmonic and harmonic stayed at the same low level as in the baseline burner. In a regular operation of the baseline burner, the low-frequency instabilities were always excited when the combustor operation was adjusted to minimize the high-frequency pulsation. The fact that even during suppression of the high-frequency mode the low frequencies remained low indicates that the VGs disrupted not only the formation of the small vortices at the sudden expansion but also the subsequent vortex interactions that lead to the larger scale vortices. The peak frequency, $Sr = 1.16$, of

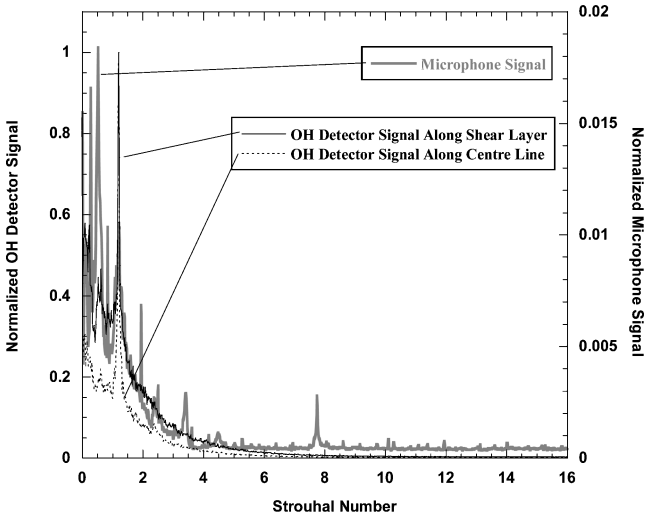

Fig. 7 Pressure and OH spectra along shear layer and centerline of burner with miniature VGs, nominal (reference) conditions.

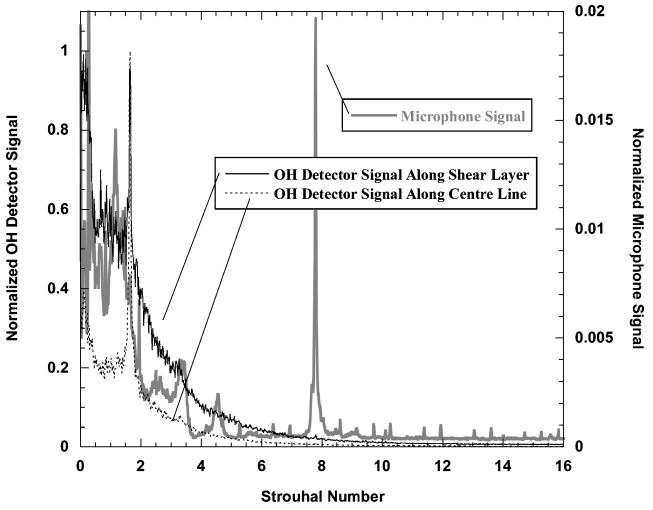

Fig. 8 Pressure and OH spectra along shear layer and centerline of burner with miniature VGs, 43% increased power relative to Fig. 7 at nominal air excess ratio.

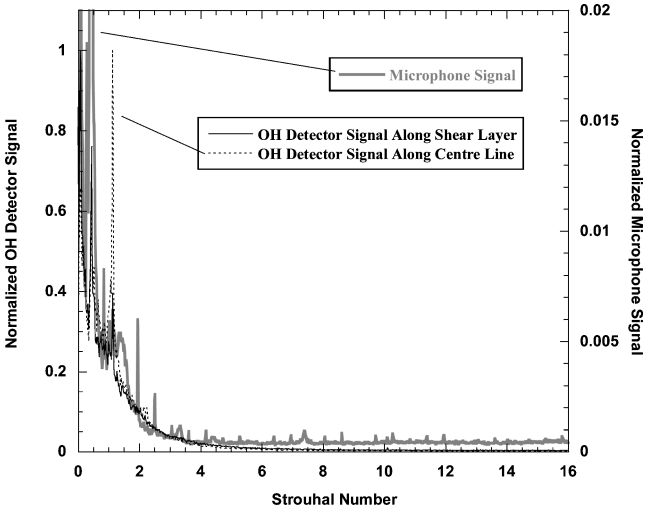

Fig. 9 Pressure and OH spectra along shear layer and centerline of burner with miniature VGs, 13% increased power, 25% lower air inlet temperature, and nominal air excess ratio.

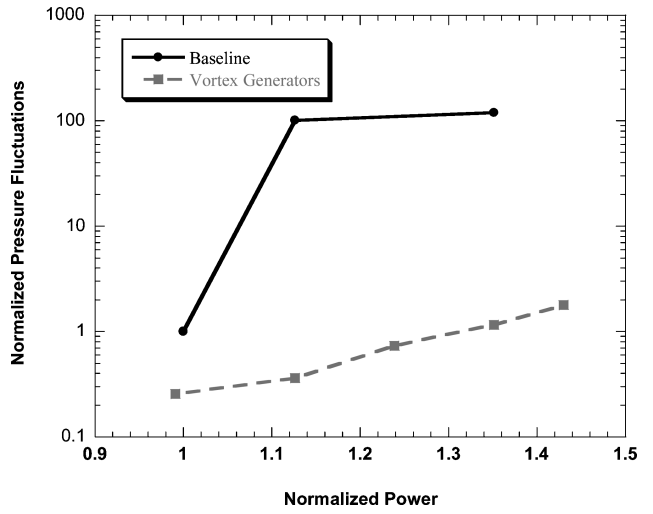

Fig. 10 Suppression of high-frequency pressure fluctuations in wide range of power settings using miniature VGs.

the OH fluctuations in the shear layer was reduced by 50%, whereas the amplitude of the same frequency increased along the centerline, signifying that the vortex breakdown instability became dominant in the heat release process.

The combustor power level was changed by modifying the air and fuel mass flow rates while maintaining a constant nominal equivalence ratio. Increased power level in the baseline burner resulted in an exponential increase in the amplitude of the high-frequency instability. When the power level was increased by 43% relative to nominal conditions, at nominal air excess ratio (Fig. 8), the high-frequency instability was kept by the VGs at a low level of 17 dB below the baseline level. In fact, it was not possible to operate the combustor without the VGs at this power level without causing structural damage to the facility. The low-frequency pressure oscillations remained at the same level as at the nominal power level. The heat release spectrum in the center showed strong activity at the $Sr = 1.16$ instability mode, which is related to the vortex breakdown at the central zone, whereas the shear layer had no discernable peaks.

Another means to excite intense high-frequency instability in the baseline burner was to reduce the inlet temperature of the combustion air. With the miniature VGs, when the air inlet temperature was reduced by 25% relative to nominal conditions with a concurrent 13% increase in power (Fig. 9), the high-frequency instability was suppressed by over 28 dB relative to the reference level and the low-frequency instabilities remained at a low level. In both cases, once the high-frequency instability was suppressed, the helical instability at $Sr = 1.16$ in the heat release became dominant on the centerline, however, at a low level and without exciting the pressure oscillations.

The effectiveness of the miniature VGs was tested in a wide range of equivalence ratios and power settings. The equivalence ratio was varied in a range of 12% below and above the nominal equivalence ratio, and the power was increased by up to 44%. In fact, without the VGs it was impossible to operate the combustor at a power excess of 35%. Pressure pulsations and OH chemiluminescence (integrated across the combustor at $x/D = 0.4$ from the burner exit) oscillations were recorded in this range of conditions. Figure 10 shows the suppression of the high-frequency thermoacoustic instabilities at increased power level. Figure 10 shows the peak level of the unstable frequency as determined from the spectral analysis. The pressure pulsations increased significantly when the power increased by at least 12% above the nominal level. In the high-amplitude range, suppression levels of 20–25 dB were measured. The high-frequency oscillations were several orders of magnitude above the low-frequency instabilities when the high mode was present. To assess the effect of the miniature VGs on the low-frequency instabilities, the acoustic boundary conditions were adjusted to eliminate this instability at the same power and inlet air temperature. The effect of the VGs on the low-frequency instability of $Sr = 0.58$ for a range of equivalence ratio is shown in Fig. 11. The low-frequency pulsation level

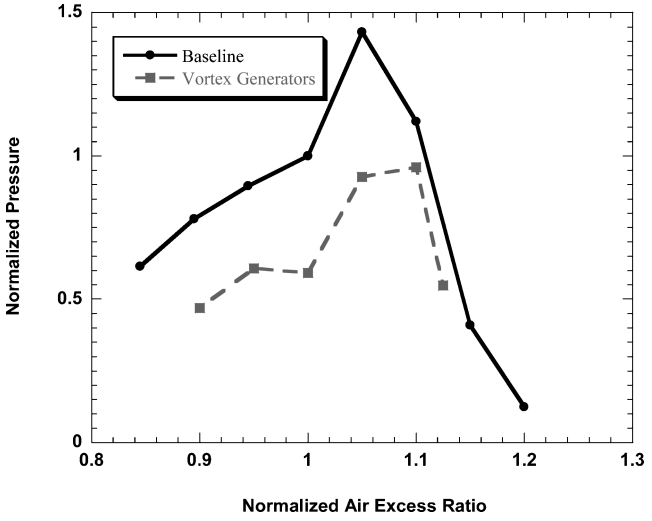

Fig. 11 Suppression of low-frequency pressure fluctuations in range of normalized air excess ratio using miniature VGs.

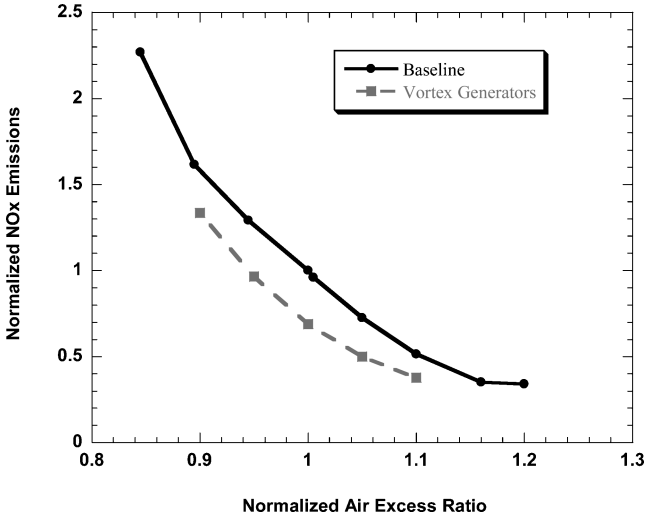

Fig. 12 Normalized NO_x emission (based on 15% O_2) vs air excess ratio with miniature VGs.

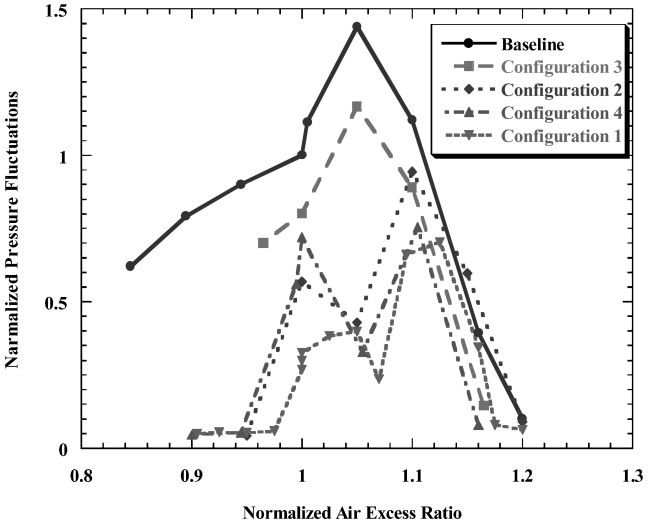

Fig. 13 Suppression of low-frequency pressure fluctuations for range of normalized air excess ratio.

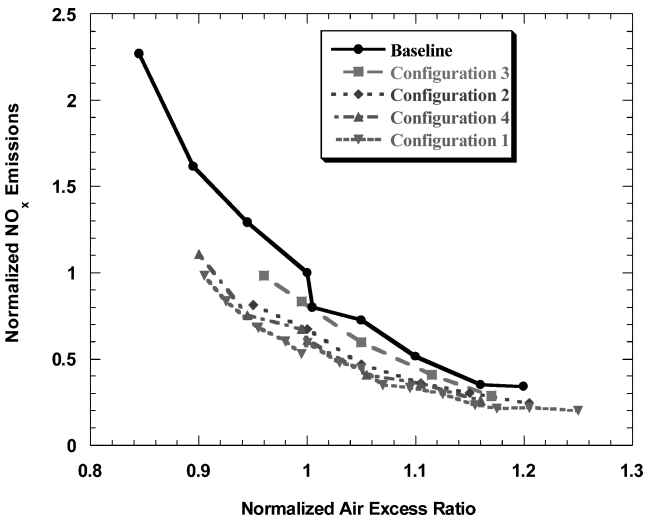

Fig. 14 NO_x emissions vs normalized air excess ratio.

was determined the same way as the high-frequency component. Suppression of up to 50% was obtained for most of the tested conditions.

Emissions of CO, NO_x, and UHC were measured for the same range of equivalence ratios as that of the thermoacoustic tests. NO_x emissions were reduced by up to 40% (Fig. 12), whereas CO and UHC were unaffected. Similar levels of suppression were achieved in a wide range of output power output from $1 < P/P_n < 1.43$. The burner could be operated at a high-power level because high-frequency pulsations were eliminated. The low-level pressure and OH oscillations as well as low NO_x persisted even when the inlet air temperature was reduced to $T/T_n = 0.74$, conditions that normally led to strong high-frequency oscillations.

VGs for Suppression of Low-Frequency Instabilities

The main purpose of the VGs described in the preceding section was to suppress the high-frequency instabilities. It was shown that at the same time the low-frequency instability was also reduced (Fig. 11). A number of different configurations were tested to assess the effect of the VGs' geometry and spacing on the low-frequency instability. The VG geometry, dimensions, and spacing are shown in Fig. 6b. The tests described here included several configurations of VGs. Two sizes of VGs were utilized, and they were installed either around the burner's exit, or in the two swirler inlet slots, or in both (Fig. 6c).

The following configurations were investigated: configuration 1, which consisted of 5 small VGs along each of the two swirler's inlet slots and 14 larger VGs around the burner's exit circumference spaced at $d_1 \approx \lambda_f/2$, where λ_f is the wave length of the low-frequency fluid dynamic instability; configuration 2, which had no VGs along the swirler inlet and 14 large circumferential VGs around the burner's exit circumference spaced at $d_2 = 0.7d_1$; configuration 3, with 5 small VGs along each of the two swirler's inlet slots, and none at the burner's exit; and configuration 4, which had no VGs along the swirler inlet and 14 large circumferential VGs around the burner's exit circumference spaced at d_1.

Pressure oscillations were recorded in addition to emissions of NO_x, CO, and UHC (Figs. 13–16). All passive control tests were compared with a baseline burner without modifications. All configurations yielded suppression for the normalized air excess ratio below 1.15. A similar trend was reported by McManus and Bowman,[6] who reported increased suppression of low-frequency fluctuations for richer mixtures.

The highest suppression of 13 dB was measured with configuration 1, which combined VGs in the swirler inlet and around the circumference. This configuration yielded also slight extension of the lean blow out limit. VGs in the swirler inlet (configuration 3) yielded marginal improvement, whereas VGs around the burner's circumference (configurations 2 and 4) exceeded the performance of configuration 1 at a normalized air excess ratio above 1.07. This configuration was less effective at richer conditions; however, it was

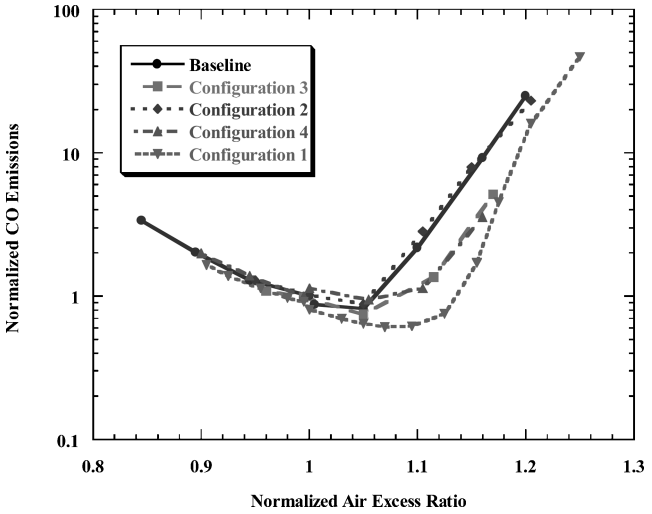

Fig. 15 CO emission (based on 15% O_2) vs normalized air excess ratio.

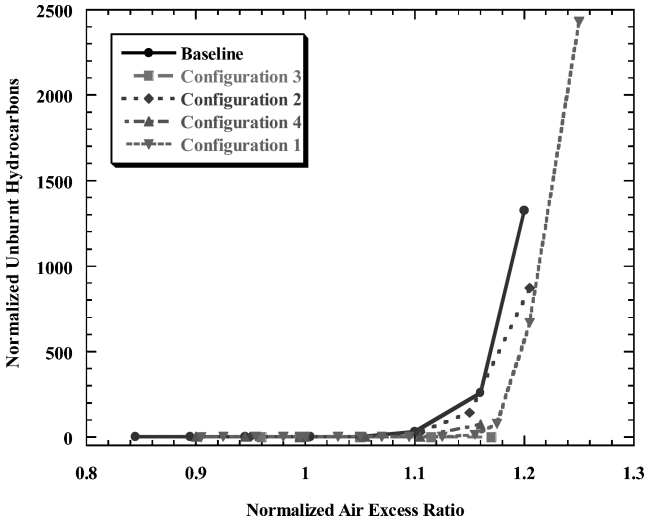

Fig. 16 UHC emission vs normalized air excess ratio.

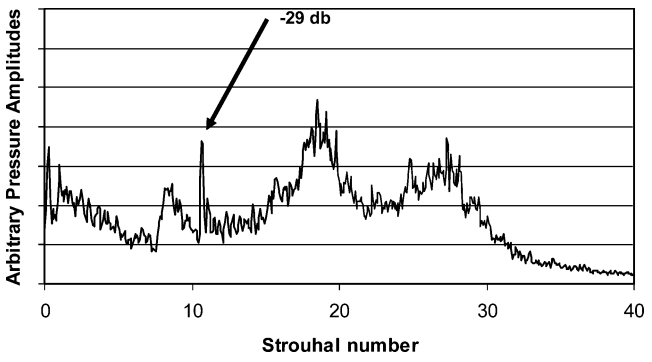

Fig. 17 Suppression of high-frequency instability in gas-turbine engine.

better than the baseline configuration. The effect of the VGs spacing at the outlet was minimal (compare configurations 2 and 4).

All configurations except the VGs in swirler inlet only (configuration 3) showed reduction of up to 40% in NO_x in the full range of normalized air excess ratio (Fig. 14). A discussion explaning the relationship between the suppression of thermoacoustic instabilities and decreased NOx production is given by Paschereit et al.[1] All configurations except configuration 2 yielded a substantial decrease in CO for normalized air excess ratio above 1.05 (Fig. 15) and UHC for normalized air excess ratio above 1.1 (Fig. 16). The highest reduction was achieved by the configuration that combined VGs in the inlet and at the circumference. The CO_2 level was identical in all configurations to the baseline burner.

To validate the laboratory experiments the miniature VGs were applied to a gas-turbine burner operating in a gas-turbine engine. Here the passive control method helped to suppress high-frequency combustion instabilities at a normalized frequency of $Sr = 10.7$ by up to 29 dB (Fig. 17).

Summary

Several modes of instabilities were identified in the experimental combustor.[1] The axisymmetric low-frequency instabilities were associated with the external recirculation zone downstream of the dump plane. The helical-low frequency instabilities were related to the central recirculation zone formed by vortex breakdown. High-frequency helical instabilities were excited when the power level was increased or when the air inlet temperature was reduced. At these conditions, the high-frequency modes dominated the thermoacoustic instability. The high-frequency oscillations were excited by the small-scale vortices that formed at the initial separating shear layer and were related to the Kelvin–Helmholtz flow instability in this region.

Distributed miniature VGs, whose size matched the boundary-layer thickness, were installed to interfere with the rollup of these vortices by inducing streamwise vorticity. The streamwise vorticity tends to interact with the circumferential vorticity causing azimuthal deformation and excitation of high-order azimuthal modes that disrupt the formation of coherent circumferential vortices. In the present case, it was shown that not only the initial vortices were affected but also the entire process that leads to the evolution of larger vortices through pairing and vortex merging was disrupted. Thermoacoustic instabilities that are excited by the periodic heat release due to the presence of coherent vortices were, thus, avoided in both the high- and low-frequency ranges. The effect was particularly significant in the high-frequency oscillations that reached high-amplitude level in the baseline burner and were suppressed by up to 28 dB by the miniature VGs. At the same time, low-frequency instabilities were reduced by 50%.

Emissions of NO_x were reduced by a factor of two in a wide range of operating conditions, whereas CO and UHC were slightly reduced. These results were confirmed also at an increased power level by up to 43% over the nominal level and with a reduction of up to 25% in inlet air temperature.

Larger VGs, whose size and spacing matched the low-frequency wavelength, were installed in the inlet to the swirler and at the burner circumference to affect the low-frequency instabilities. Suppression of the pressure oscillations by 13 dB with substantial reduction in NO_x, CO, and UHC was achieved by a combination of VGs in the swirler inlet and around the outlet. VGs at the inlet or outlet only were not as effective. The increased size of the VGs improved their effect on the low-frequency instability but rendered them ineffective to high-frequency instabilities. Spacing of the VGs at the outlet was not consequential.

The results obtained here in a laboratory combustor operating at atmospheric pressure were later confirmed in high-pressure engine combustion tests.

Acknowledgment

The authors acknowledge the support of Wolfgang Weisenstein, ABB (Switzerland), Ltd., to carry out this research, which was performed at ABB Corporate Research in Baden-Daetwil, Switzerland.

References

[1] Paschereit, C. O., Gutmark, E., and Weisenstein, W., "Structure and Control of Thermoacoustic Instabilities in a Gas-Turbine Combustor," *Combustion Science and Technology*, Vol. 138, No. 1, 1998, pp. 213–232.

[2] Schadow, K. C., and Gutmark, E., "Combustion Instability Related to Vortex Shedding in Dump Combustors and Their Passive Control," *Progress in Energy and Combustion Science*, Vol. 18, No. 2, 1992, pp. 117–132.

[3] McManus, K. R., Poinsot, T., and Candel, S. M., "A Review of Active Control of Combustion Instabilities," *Progress in Energy and Combustion Science*, Vol. 19, No. 1, 1993, pp. 1–29.

[4]Paschereit, C. O., Gutmark, E., and Weisenstein, W., "Coherent Structures in Swirling Flows and Their Role in Acoustic Combustion Control," *Physics of Fluids*, Vol. 11, No. 9, 1999, pp. 2667–2678.

[5]Gutmark, E., and Grinstein, F., "Mixing in Non-Circular Jets," *Annual Review of Fluid Mechanics*, Vol. 31, 1999, pp. 239–272.

[6]McManus, K. R., and Bowman, C. T., "Effects of Controlling Vortex Dynamics on the Performance of a Dump Combustor," *Twenty-Third Symposium (International) on Combustion*, Combustion Inst., Pittsburgh, PA, 1990, pp. 1093–1099.

[7]Doebbeling, K., Eroglu, A., Joos, F., and Hellat, J., "Novel Technologies for Natural Gas Combustion in Turbine Systems," *Eurogas-99, European Applied Research Conference on Natural Gas*, Ruhr-Universität, Bochum, Germany, 1999, pp. 75–81.

[8]Cattolica, R. J., "OH Radical Non-Equilibrium in Methane–Air Flat Flames," *Combustion and Flame*, Vol. 44, No. 1–3, 1982, pp. 43–59.

[9]Ho, C., and Huerre, P., "Perturbed Free Shear Layers," *Annual Review of Fluid Mechanics*, Vol. 16, 1984, pp. 365–424.

[10]Paschereit, C. O., Wygnanski, I., and Fiedler, H. E., "Experimental Investigation of Subharmonic Resonance in an Axisymmetric Jet," *Journal of Fluid Mechanics*, Vol. 283, 1995, pp. 365–407.

[11]Paschereit, C. O., Gutmark, E., and Weisenstein, W., "Control of Axisymmetric Combustion Instability Modes by Antisymmetric Fuel Injection," *17th International Colloquium on the Dynamics of Explosions and Reactive Systems*, Heidelberg Univ., Heidelberg, Germany, 1999, p. 83.

R. Lucht
Associate Editor